Investigation of far-infrared vibrational modes in polynucleotides

J. W. Powell, G. S. Edwards,* L. Genzel, F. Kremer,† and A. Wittlin‡
Max-Planck-Institut für Festkörperforschung, Heisenbergstrasse 1, Postfach 80 06 65, D-7000 Stuttgart 80, Federal Republic of Germany

W. Kubasek and W. Peticolas
Department of Chemistry, University of Oregon, Eugene, Oregon 97403
(Received 26 November 1986)

Far-infrared measurements (40—500 cm^{-1}) of vacuum-dried, free-standing, unoriented films of the polynucleotides poly(dA)·poly(dT), poly(dA-dT)·poly(dA-dT), and poly(dG)·poly(dC) and the ribonucleotide poly(rA)·poly(rU) under various salting conditions are reported. Spectral features that depend on temperature, crystallinity, and salting conditions have been observed. Of most interest are four sharp bands near 63, 83, 100, and 110 cm^{-1} in polycrystalline poly(dA)·poly(dT). These low-frequency (<240 cm^{-1}) observations are discussed in terms of a lattice-dynamical model of homopolymer DNA.

I. INTRODUCTION

In this paper we describe and model our observations that concern the salting and crystallinity dependence of infrared (IR) -active modes between 40 and 500 cm^{-1} in polynucleotide films. The low-frequency (40—240 cm^{-1}) modes in sequence-defined DNA are emphasized.

In order to place our far-infrared (FIR) measurements on polynucleotides in the proper perspective with the growing field of low-frequency dynamics of DNA, it is necessary to briefly review the development of a portion of the theoretical and experimental work that has taken place in the last several years. Theoretical effort has been expended in the following directions: lattice dynamics,[1] molecular dynamics,[2,3] and nonlinear dynamics.[4,5] The first lattice-dynamical treatment of a nucleic acid molecule was presented by Eyster and Prohofsky in 1974 who considered an isolated helical duplex of homopolymer RNA.[6,7] Dynamically, all atoms of the unit cell except the hydrogen atoms were taken into account. High-frequency Raman data provided many of the force constants required. When comparison with acoustic data became possible with the measurements of Maret *et al.*[8] in 1979 and later of Hakim *et al.*,[9] then the model could be refined by including long-range nonbonded interactions. This refined lattice-dynamical theory made several predictions that compare favorably with subsequent observations.[1]

In the seminal study on the FIR absorption of nucleic acids, Beetz and Ascarelli[10] measured poly(I)·poly(C), various nitrogenous bases, and nucleosides in the region 25—500 cm^{-1}. In addition to reporting the hydration dependence of a 45-cm^{-1} mode, they observed features in the region $\sim$300—500 cm^{-1} that were assigned to the ribose ring vibrations. Calculations of poly(rA)·poly(rU) (Ref. 7) were in reasonable agreement with the poly(I)·poly(C) data.[10]

Very recently Wittlin *et al.*[11] measured the transmission spectrum of oriented films of Li and Na calf thymus DNA from 3 to 450 cm^{-1} in the temperature range 5—300 K. They also observed a 45-cm^{-1} mode in addition to four other low-frequency features and traced its softening with hydration. A simple lattice-dynamical model and the resulting eigenvectors were presented. This model treated part of the hydration softening by means of water mass loading. With this model the 45-cm^{-1} mode was assigned to the eigenvector in which the base pairs vibrate in phase and in countermotion to the two sugar-phosphate backbones along the helical axis.

In addition to the work in the FIR, microwave studies have been made. In 1984 Edwards *et al.*[12] demonstrated the existence of longitudinal acoustic resonances in the low-gigahertz region in solutions of monodisperse DNA of definite length. This result was predicted by Kohli *et al.*[13] These observations imply that the long-wavelength longitudinal acoustic modes of DNA are subject to significantly less solvent damping than previously thought.[14,15] One other model[16] which explains various parts of these data has recently been proposed.

Inelastic light-scattering on oriented films and fibers has made a significant contribution to the understanding of the dynamics of DNA. The lowest-frequency feature which has been observed is a sharp q vector independent mode near 600 MHz (Ref. 17) that was tentatively assigned to a defect resonance associated with the terminus of the DNA molecule.[18] The idea that low-lying Raman bands could be related to the A-to-B conformation shift in DNA has been studied theoretically. Prohofsky and co-workers[1,19] treated the conformation shift as a soft-mode mediated displacive phase transition, and Martin[20] used a classical double-well oscillator to model the A-to-B transition by taking into account the low-frequency Raman observation of Painter and co-workers.[21] Recently it has been suggested[22] that the existence of strong interhelical interactions are a significant factor in the dynamics of this conformation shift. Using low-frequency Raman scattering, Urabe and Tominaga[23] and DeMarco *et al.*[22] have observed the softening of a Raman mode near 25

cm^{-1} in Na-DNA which may be closely related in character to the lowest-lying Raman mode (12 cm^{-1} in *B*-DNA) observed by Lindsay and co-workers.[24] In Na-DNA the softening increases substantially at the relative humidity where the x-ray fiber diffraction patterns indicate change from *A* to *B* conformation.[25] Tominaga *et al.*[26] measured optical modes in DNA gels near 30 cm^{-1} at low temperatures and observed both Raman intensity and frequency changes with temperature. These changes were attributed to a variable coupling of DNA vibrations to relaxational modes of water. Recently Tao *et al.*[27] measured DNA films with Brillouin scattering at low temperatures and constructed a coupling model similar to that of Tominaga *et al.*[26] to account for the dependence of Brillouin linewidths on hydration. A recent paper by Lee *et al.*[28] presents comprehensive results of Brillouin scattering and physical characterization measurements on highly oriented DNA films of both Na and Li salts and a model for softening of interhelical elastic constants.

It has become apparent from x-ray diffraction studies that under certain circumstances specific base sequences can cause nonclassical nucleic acid tertiary structures.[29,30] The homopolymer poly(dA)·poly(dT) exemplifies this point. The full magnitude of the structural variability of this homopolymer was realized in 1984. At that time Arnott *et al.*[30] postulated a "heteronomous" structure in which one strand is *A*-like and the other is *B*-like. This heteronomous structure analysis was supported by Raman measurements of Thomas and Peticolas[31] on poly(dA)·poly(dT) in the neighborhood of 800 cm^{-1}. They found evidence of both C3′ (*A* family) and C2′ (*B* family) furanose ring conformations. Jolles *et al.*[32] used ultraviolet resonance Raman scattering to demonstrate that only one strand of poly(dA)·poly(dT), that of adenine, has an *A*-form sugar pucker, thereby adding credibility to the postulated heteronomous structure. Arnott[33] has also pointed out that it is possible for poly(dA)·poly(dT) to disproportionate into triple and single helices under conditions of high salt concentration and low humidity. Further evidence of the unusual structure and dynamics of poly(dA)·poly(dT) was obtained by Cantor *et al.*[34] using circular dichroism and by Wartell and Harrell[35] using high-frequency Raman spectroscopy.

Poly(dA)·poly(dT) has been demonstrated to have a strong effect on the curvature of DNA in solution by polyacrylamide gel electrophoresis.[36–39]

II. EXPERIMENTAL

A. Sample preparation and characterization

The four polynucleotides poly(dA)·poly(dT) (lot number 1147-04 671), poly(dG)·poly(dC) (lot number 67C-03 962), poly(dA-dT)·poly(dA-dT) (lot number 74F-0066), and poly(rA)·poly(rU) (lot number 21F-03 381) were purchased from Sigma Chemicals. All solutions were prepared using twice glass distilled water. The unoriented films were prepared by adding water to the supplier lyphozilized DNA. In this manner the DNA hydrated to uniform gel in a 100% relative humidity environment for 24 hours. This gelation procedure prevented the formation of inhomogeneities in the film, which otherwise would be introduced by mechanical stirring methods. Films were formed by slowly drying the gel in a dessicator for another 24 hours.

Films of different salt contents were prepared using a technique similar to that of Rupprecht and Forslind.[40] Samples were subjected to FIR measurements at each of five concentrations of NaCl in the dialyzing solution 0*M*, 0.01*M*, 0.1*M*, 1.0*M*, and saturated. In order to achieve reproducibility in sample preparation we established a concentration reference point in our films by first dialyzing our samples against 100 ml of 73% (v/v) ethanol and 27% (v/v) water for approximately 15 hours. This nondissolving solution was replaced once during this period. Samples which were only dialyzed against this solution are referred to as minimal salt films. Salted films were obtained by dialyzing the minimal salt films in 73% ethanol and 27% salt solution at the stated molarity. Additionally, samples were measured whose salt content was not altered as received from the supplier. Such samples are referred to as supplier salt films. The salt content of these films was estimated to be similar to that of our 1.0*M* samples by comparison of FIR spectra of films of known dialyzing solutions.

In order to establish the extent of crystallization in the films, x-ray patterns were obtained using nickel filtered CuKα radiation. The results of the x-ray analysis indicated that all the films were nearly amorphous. Only in the case of minimal salt poly(dA)·poly(dT) did the diffraction data show strong polycrystalline character. Furthermore, only saturated salt films gave diffraction patterns which revealed the presence of salt crystals.

As mentioned in the Introduction poly(dA)·poly(dT) has been observed in a disproportionated conformation[29] as well as in a heteronomous structure.[30] We have compared our poly(dA)·poly(dT) fiber diffraction patterns with Arnott's[33] double helical patterns and it was found that our poly(dA)·poly(dT) films are heteronomous.

B. Spectroscopy

Transmission measurements were made on a Bruker IFS 113A rapid scan Fourier-transform infrared spectrometer between 40 and 500 cm^{-1}. The resolution was either 0.5 or 2.0 cm^{-1}, depending on the spectral range measured. The spectrometer was equipped with a liquid helium cooled germanium bolometer. All the measurements were made in vacuum to prevent the presence of water rotational absorption lines in our DNA spectra. Presently it is not possible to make meaningful measurements at frequencies lower than 40 cm^{-1} because the polynucleotide samples are too fragile to form the sufficiently thick and large diameter films required to provide adequate absorption below 40 cm^{-1}. It is also noteworthy that one cannot obtain reliable results from DNA solutions since water absorption completely dominates the spectra.

The optical properties (refractive index n and extinction coefficient k) of the samples were determined from the transmission spectra using an iterative process. The analysis uses the expression for the transmission through

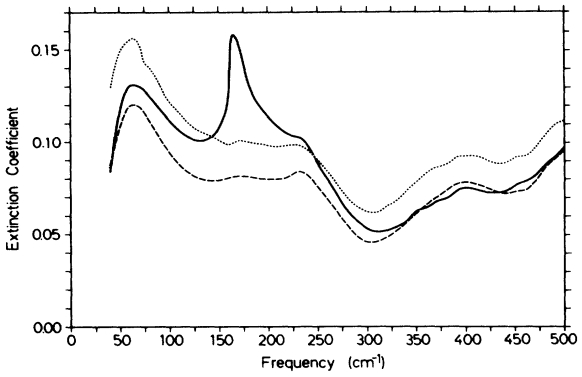

FIG. 1. Extinction coefficient spectra for vacuum-dried poly(dG)·poly(dC) for different salt concentrations and temperatures at 2 cm^{-1} resolution. The solid curve corresponds to a room-temperature measurement on a film which has been dialyzed against a saturated NaCl solution. The long- and short-dashed curves correspond to 5- and 300-K measurements, respectively, on films which had been dialyzed against 1.0 M NaCl.

a lamella to calculate a provisional extinction coefficient spectrum in terms of the thickness, a preliminary-constant refractive index, and the transmission data. Spectra distortion (channeled spectra) due to multiple interference effects were not observed experimentally due to variations in optical thickness of the films. The refractive index of natural DNA at relative humidity 1% near 6 cm^{-1} was measured to be 1.9 using a polarizing millimeter wave interferometer.[41] The iterative procedure continues by fitting the extinction coefficient as obtained from Eqs. (1) and (2) below to the extinction coefficient obtained using the original transmission data:

$$\epsilon(\nu)=\epsilon_1+i\epsilon_2=\epsilon_\infty+\sum_j \frac{S_j\nu_j^2}{\nu_j^2-\nu^2-i\nu\gamma_j} , \quad (1)$$

where ϵ is the complex dielectric function, ν represents

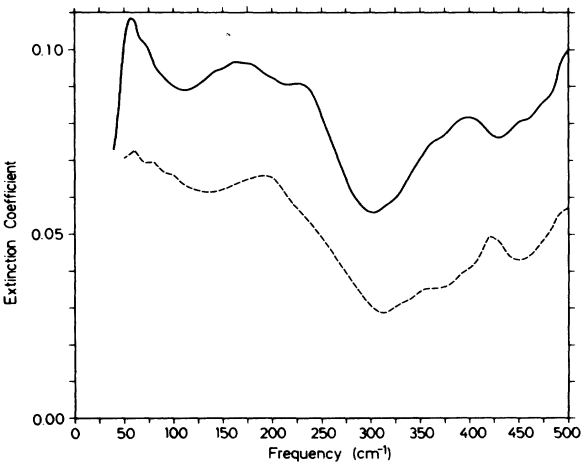

FIG. 2. Extinction coefficient spectra of vacuum-dried and minimal salt films of poly(dG)·poly(dC) and poly(dA-dT)·poly(dA-dT), both measured at 300 K with a resolution of 2 cm^{-1}. The solid line corresponds to poly(dG)·poly(dC), the dashed line corresponds to poly(dA-dT)·poly(dA-dT).

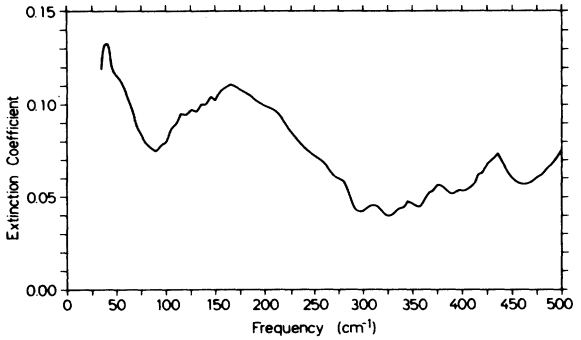

FIG. 3. Extinction coefficient spectrum for vacuum-dried poly(rA)·poly(rU) supplier salt film (corresponding dialyzing solution approximately 1 M NaCl) measured at 5 K with a 2-cm^{-1} resolution.

the frequency in wave numbers, ϵ_1 and ϵ_2 are the real and imaginary parts of ϵ, ϵ_∞ is the high-frequency dielectric constant, and S_j, ν_j, and γ_j are the oscillator strength, eigenfrequency, and full width at half maximum, respectively. The complex index of refraction is defined as

$$N(\nu)=n+ik, \quad \epsilon_1=n^2-k^2, \quad \epsilon_2=2nk . \quad (2)$$

The final extinction coefficient spectrum is the result of recalculating k, this time using the frequency dependent refractive index obtained from the fit described above.

III. RESULTS

The results of our measurements and data analysis are presented in Figs. 1–9. Detailed explanations are deferred to the theory and discussion section. The frequencies of spectral features of every figure are listed in Table I. Additionally, Table II presents published infrared frequencies of DNA and RNA for comparison with the present data. Figure 1 permits a comparison of poly(dG)·poly(dC) spectra obtained under different salting and temperature conditions. The effects of different salting conditions are seen by comparing the solid and short-

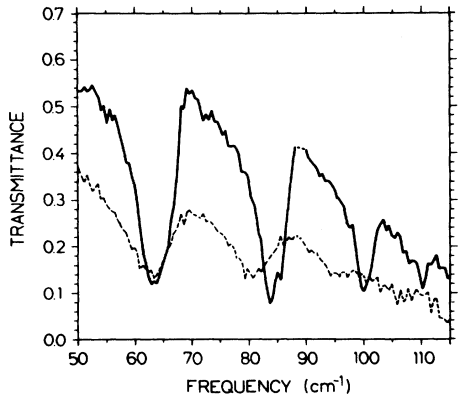

FIG. 4. Transmission spectrum of minimal salt, vacuum-dried Na-poly(dA)·poly(dT). The solid curve represents the data at 7 K whereas the dashed curve represents the data at room temperature. An instrumental artifact at 90 cm^{-1} has been replaced by a few dots.

TABLE I. Observed frequencies for various polynucleotides. All numbers are in units of cm^{-1}.

Poly(dA)·poly(dT)			Poly(rA)·poly(rU)	Poly(dG)·poly(dC)				Poly(dA-dT)·poly(dA-dT)
Fig. 4	Figs. 4 and 5	Fig. 6	Fig. 3	Fig. 1	Fig. 1	Fig. 1	Fig. 2	Fig. 2
Min. salt[a]	Min. salt	Min. salt	Supplier	Supplier	Supplier	Saturated	Min. salt	Min. salt
300 K	7 K	300 K	5 K	5 K	300 K	300 K	300 K	300 K
62	63	62	40	65	65	65	56	60
80	83	80	56		84		74	80
95	86	96	96					100
106	100		105					
	110	122						
		136	166				142	
		170	212			170	160	
		214	260				181	195
		238	281	231	233	233	235	247

[a]Min. salt is an abbreviation for minimum salt. Refer to Sec. II A in text.

dashed traces whereas one can see the temperature effects by comparing the short- and long-dashed traces. Both the temperature and salt effects in poly(dG)·poly(dC) are characteristic of all films measured. All saturated salt films (including natural DNA) show a strong band at 170 cm^{-1}, and generally low-temperature measurements increase the transmission over the entire spectral range. Spectra of minimal salt poly(dA-dT)·poly(dA-dT) and poly(dG)·poly(dC) are displayed in Fig. 2. A poly(rA)·poly(rU) spectrum is presented in Fig. 3, and it is noteworthy that this spectrum shows many similarities to the data of Beetz and Ascarelli.[10]

Data concerning poly(dA)·poly(dT) are shown in Figs. 4–6. Transmission data for a minimal salt, highly polycrystalline film at two widely separated temperatures (7 and 300 K) are shown in Fig. 4. These data are displayed in transmission to emphasize the change of half-width and band position with temperature. Figure 5 shows the extinction coefficient spectrum for the 7 K curve in Fig. 4. The salt dependence in the low-concentration regime for the film of Fig. 4 is shown in Fig. 6. The solid curve in Fig. 6 came from a film which gave a highly polycrystalline x-ray fiber diffraction pattern. Other samples of minimal salt poly(dA)·poly(dT) did not necessarily give such sharp data for both x-ray diffraction patterns and FIR spectra. Nevertheless, even films of lower polycrystallinity showed the same features above 120 cm^{-1} but more weakly.

TABLE II. Infrared frequencies in DNA and RNA below 300 cm^{-1} observed by other groups.

Infrared			
Frequency cm^{-1}	Type	Condition	Ref.
45	poly(I)·poly(c)	low salt	10
100	RNA	$T=56$ K	
170			
205			
45	Li-DNA	low salt	11
111		$T=5$ K	
195			
41	Na-DNA	low salt	11
100		$T=5$ K	
200			

IV. THEORY AND DISCUSSION

The lattice dynamics of DNA has been worked out by Prohofsky and co-workers.[1,7,13,19] It is the most accurate and detailed theory for DNA since it takes into account the helical structure and all atoms besides hydrogen in the unit cell. The theory includes both short- and long-range interactions. The model, therefore, has quite a large number of parameters. Our present study attempts only to assign the spectral features of poly(dA)·poly(dT) (Figs. 5 and 6) below 300 cm^{-1}. We have chosen, therefore, a much simpler model which is an extended version of one previously presented.[11] It is based on an isolated homopolymer DNA duplex with an unraveled structure as shown in Fig. 7. Since we are interested only in low-frequency modes, we consider eight particles per unit cell where each particle represents one of the following molecular subunits: base, sugar ring, phosphate, and counterion. These subunits are connected by harmonic nearest-neighbor force constants for each of the three mutually orthogonal displacement directions ξ, η, and ζ. ζ represents the direction of the chain axis, ξ and η are the directions parallel and perpendicular to the hydrogen

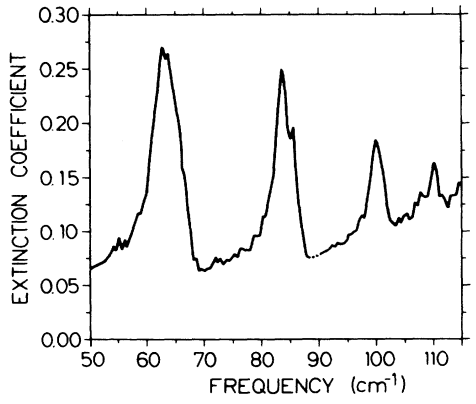

FIG. 5. Extinction coefficient spectrum of minimal salt vacuum-dried poly(dA)·poly(dT) at 7 K with a resolution of 0.5 cm^{-1}. This spectrum was obtained using the 7-K data in Fig. 4.

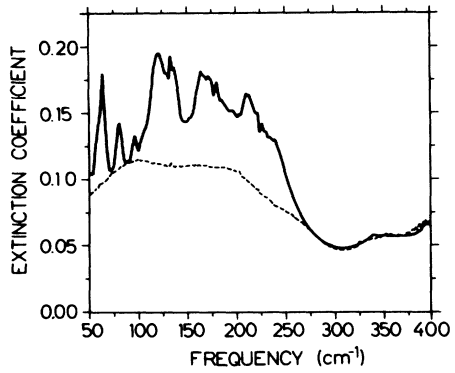

FIG. 6. Extinction coefficient spectra of vacuum-dried poly(dA)·poly(dT) at different salt concentrations, room temperature, and 2.0-cm^{-1} resolution. The top curve corresponds to a minimal salt film and the bottom curve to a sample which had been dialyzed against 0.1 M NaCl.

bonds between the bases, respectively (Fig. 7). In the model we consider the motions in the three directions as being decoupled. The particles of the model have known masses and carry charges. We consider lattice waves propagating parallel to the chain axis.

It should be noted that an unraveled DNA model has several drawbacks as compared to a model which contains the correct helical symmetry. The failures are especially severe towards the edge of the Brillouin zone because the short wavelength there probes the details of the structure more than at the zone center. Similarly, the branches at higher frequencies will be more sensitive to the details of the model. The present model, furthermore, fails in not describing torsional motions. The eigenfrequencies with their associated eigenvectors are grouped onto eight branches for each displacement direction, with one branch

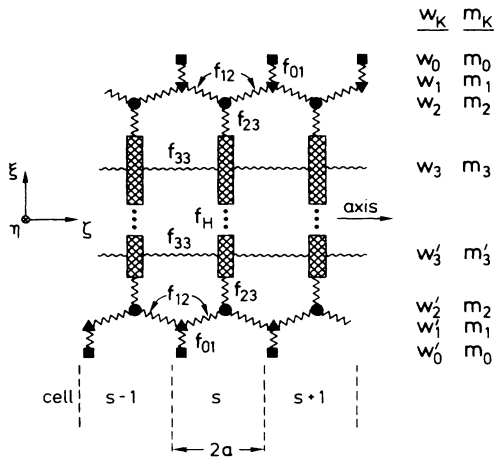

FIG. 7. Lattice model of Na-poly(dA)·poly(dT): m_0, m_1, m_2, m_3, and m_3' represent the mass of counterion, phosphate group, sugar ring, and mass of adenine and thymine, respectively. f_{01}, f_{12}, f_{23}, f_{33}, and f_H represent effective force constants. Cross-hatching indicates the bases: the larger base represents adenine and the smaller thymine. The w's represent the displacements in the three mutually perpendicular directions ξ, η, and ζ.

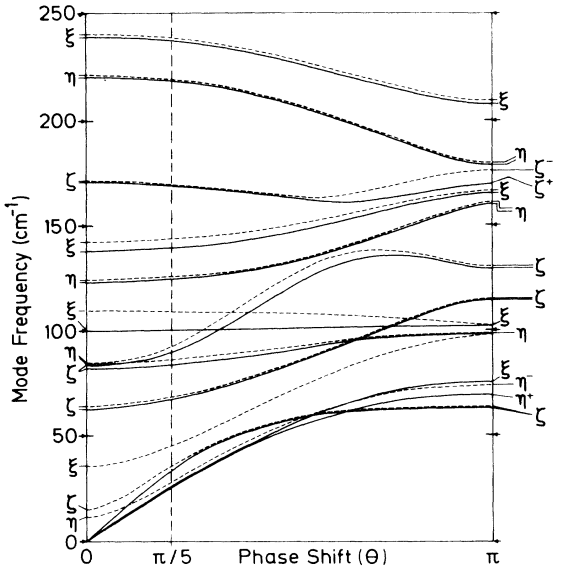

FIG. 8. Calculated dispersion curves for Na-poly(dA)·poly(dT); plus modes, solid curves; minus modes, dashed curves. The parameters for this calculation are given in Table III. ξ, η, and ζ refer to the directions indicated in Fig. 7.

being of the acoustical type and the remainder being of the optical type. The eigenfrequencies for each branch are functions of the cell-to-cell phase shift θ ($0 \leq \Theta \leq \pi$). The wave vector of our ladder model is $\theta/2a$ where $2a$ is the lattice spacing. The experimentally observed IR and Raman bands arise from the ζ modes only at $\theta=0$. Due to the helix period of ten base pairs for poly(dA)·poly(dT), the ξ and η modes will in reality be IR or Raman active at $\theta=\pi/5$. Since the structure of the polymer shows a small inclination of the base planes to the normal of the helix axis,[29] one can also expect some activity of the ξ modes at $\theta=0$. In addition this inclination means that the decoupling of the motions in the model is an approximation.

The experimentally observed IR bands are characterized by their frequencies and oscillator strengths. To reinforce our assignment, the measured oscillator strengths were compared with values calculated from the eigenvectors and the charge distribution within the unit cell.

The model we use has a set of force constants f_{01}, f_{12}, f_{23}, f_{33}, and f_H for each direction. The lattice spacing $2a$ is known from x-ray measurements[30] and the longitudinal sound velocity V_S in ζ direction is taken from Brillouin scattering measurements on oriented fibers of natural DNA.[9] The transverse sound velocity can only be estimated according to usual ratios of transverse-to-longitudinal sound speeds in solids.[42] The present lattice-dynamical model yields an expression for the sound velocity:[11]

$$V_S = 2a \left[\frac{f_{33} + 0.5 f_{12}}{M} \right]^{1/2}, \tag{3}$$

where M is the half unit-cell mass. From this expression one obtains f_{33} as a function of f_{12}, and f_{12} is fitted to observations. In fact, this is an important point because

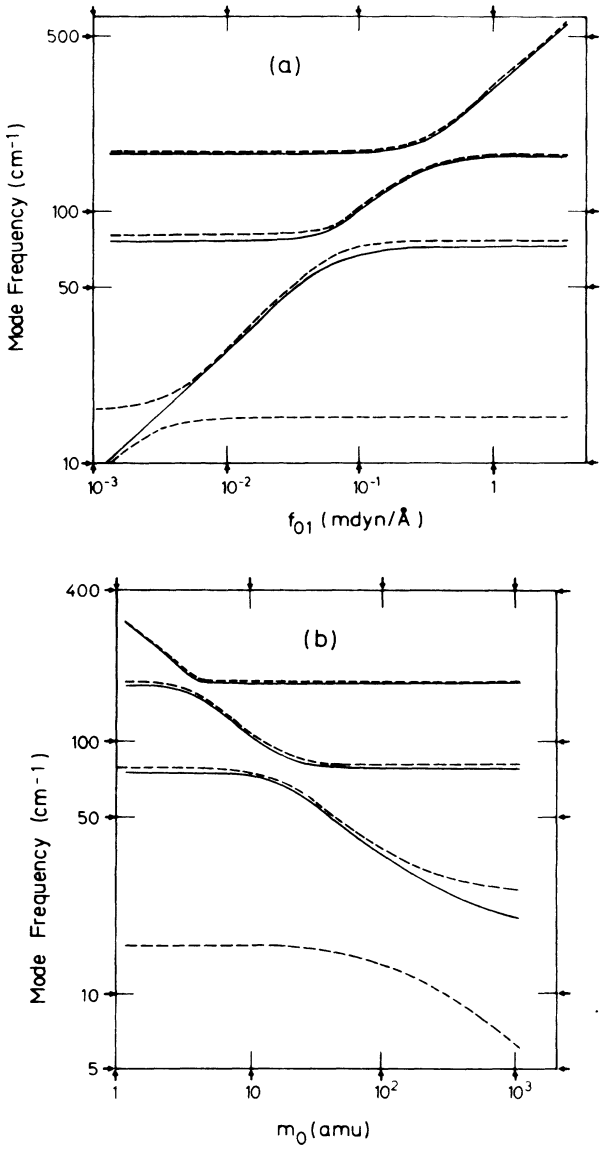

FIG. 9. (a) Calculated f_{01} softening curves for the Na-poly(dA)·poly(dT) ζ modes. (b) Calculated mass loading curves for Na-poly(dA)·poly(dT) ζ modes at the constant f_{01} listed in Table III. In both (a) and (b) dotted and solid curves represent the minus and plus modes, respectively.

f_{33} cannot be obtained from measured optical modes since it is not involved in these motions. Therefore, we are left with four unknown force constants for each direction which have to be adjusted to model the observed IR and Raman frequencies in an assignment which takes into account the oscillator strength.

A straightforward assignment is possible for the lowest optical Raman modes which have been observed at low humidity at 15, 26, and 35 cm^{-1}.[1] These modes must involve motion with the highest possible effective mass and with the lowest force constants. These modes are essentially counter vibrations of one chain of the duplex against the other in which f_H is the restoring force constant. In the low-frequency limit our model yields[11]

$$\omega_R^2 \cong \frac{f_H}{0.5M} , \tag{4}$$

where $0.5M$ is the reduced mass of the motion described. We assign the 35-cm^{-1} mode to the ξ direction because f_H in this direction is a stretch force constant. The 15- and 26-cm^{-1} Raman modes are then attributed to the ζ and η direction, respectively (see Fig. 8). The ξ and η Raman modes can in fact occur at $\theta=0$ and at $\theta=\pi/5$. Only a detailed calculation of the scattering can show which of these two cases is the more important one. Qualitatively, one would expect that the $\theta=\pi/5$ modes yield stronger Raman activity because of the greater relative motion of neighboring particles.

Due to the coupling of the two chains of the duplex by means of the hydrogen bonds, we will obtain Davydov paired branches. In fact, the above discussed Raman modes are Davydov-split from the corresponding acoustic branches. For each direction we are left with three Davydov pairs of optic branches. Each pair has a branch in which the corresponding particles of the two chains move in phase (plus modes) and a branch in which they move out of phase (minus modes). The plus modes are always lower in frequency than the corresponding minus modes. It turns out that there are strong constraints in grouping the branch pairs due to mode repulsion within the Brillouin zone.

We assign the observed IR modes at 63 and 83 cm^{-1} to ζ modes (see Fig. 8) because of their high oscillator strengths and their relatively low frequencies. The corresponding minus modes are too weakly split to be resolved experimentally. The mentioned constraints do not allow us to put the third ζ-mode pair lower than 170 cm^{-1}. Since the ξ modes involve a force constant f_{23} which has a stronger stretch component than for ζ and η modes, we assign the lowest ξ pair to the 100 cm^{-1} (plus mode) and 110 cm^{-1} (minus mode) at $\theta=\pi/5$. The relatively large splitting of this pair is caused by the relatively large force constant f_H. The two other ξ-mode pairs are then placed at 140 and 238 cm^{-1}. The lowest η-mode pair should have a lower frequency than the lowest ξ-mode pair. Since the experiment at low temperatures (Figs. 4 and 5) yielded a weak sideband on the 83-cm^{-1} ζ mode, we assign this sideband at 86 cm^{-1} to the lowest η^+ mode. The other two η-mode pairs are then placed at 126 and 220 cm^{-1}.

With this assignment, the force constants listed in Table III are determined. We cannot claim that our assignment is unique. This is especially true in the frequency range above 110 cm^{-1} where complex groups of bands appear (see Fig. 6—solid line) which would allow for slight changes in the assignment. We have estimated the effect of interhelical forces by connecting two duplexes through force constants $f_\perp$ between all phosphate counterion groups and taking account of the Brillouin scattering measurements[9] of the sound velocity perpendicular to the helix axis in an oriented fiber. We find that $f_\perp$ would be of the order of 0.1 mdyn/Å which compares favorably with the value of the interhelical elastic constant which Lee *et al.*[28] calculated from Brillouin scattering measurements. Comparing $f_\perp$ with the effective force constants

TABLE III. Na-poly(dA)·poly(dT) lattice-dynamics input data.

Data	ζ modes $\parallel$ modes	ξ modes $\perp$ modes	η modes $\perp$ modes
m_0[a]	23	23	23
m_1	95	95	95
m_2	83	83	83
m_3	134	134	134
m_3'	125	125	125
f_{01}[b]	0.063	0.190	0.174
f_{12}	0.322	0.584	0.553
f_{23}	0.300	0.757	0.435
f_{33}	0.451	0.129	0.029
f_h	0.024	0.156	0.013
V_s[c]	3.4	2.4	2.4
$2a$[d]	3.23	3.23	3.23

[a]Masses are in units of amu.
[b]Effective force constant in units of mdyn/Å.
[c]Velocity in units of 10^5 cm/s.
[d]Unit-cell lattice constant in units of Å.

for the ξ and η modes in Table III, it is seen that $f_\perp$ is relatively small and that the assumption of decoupling of duplexes within a solid is reasonable, except for the modes which involve the effective force constant f_{01}, especially in the ξ direction. The eigenvectors of the assigned modes are listed in Table IV for the case of the zone center ζ modes. The 63- and 83-cm^{-1} plus modes are counter vibrations of the base against the sugar-phosphate backbones. They are distinguished by the relative displacement of the counterion which is in phase with the phosphate for the 63-cm^{-1} mode in contrast to the out-of-phase motion for the 83-cm^{-1} mode. The 170-cm^{-1} mode is a backbone vibration in which the sugars essentially move against the phosphates. This mode is thus insensitive to the mass and the coupling of the counterion. It should be noted, however, that the force constant f_{01} softens critically the 63-cm^{-1} plus mode under simulated dissociation of the counterion. This is demonstrated in Fig. 9(a) where the $\theta=0$ lattice modes for the ζ direction are plotted against f_{01}. For vanishing f_{01} the mode originally at 63 cm^{-1} goes to zero along with the Raman mode originally at 15 cm^{-1}.

The minus mode originally at 65 cm^{-1} now becomes a Raman mode slightly above 15 cm^{-1} with an eigenvector which is identical to that of the former 15-cm^{-1} Raman mode but with the m_0 missing because the eight-particle unit cell has now become a six-particle unit cell of the model. It can also be seen that the 84-cm^{-1} modes take over the role of the original 63-cm^{-1} modes in the same way as f_{01} approaches zero.

In Fig. 9(b) we display the effects of mass loading on the calculated dynamics of poly(dA)·poly(dT). This constant f_{01} plot bears similarities to the softening curve of Fig. 9(a). In both cases the Raman modes soften as expected, but the Raman mode of higher frequency softens to nearly the same frequency which the lower mode had before the onset of softening but not further. Experimentally it would be very difficult to determine which branching one was on, and it might appear that the mode was not softening at all. In fact this situation may provide a deeper understanding of the behavior of the 85-cm^{-1} Raman mode observed both in solid and solution by Urabe and Tominaga[43] as well as the 34-cm^{-1} hydration independent Raman band observed by Lindsay and coworkers.[1]

Prohofsky and co-workers[1] have shown that the poly(dG)·poly(dC) modes at 85 and 129 cm^{-1} slightly soften if the two strands of the helix duplex separate ("melting"). For our poly(dA)·poly(dT) calculations similar effects occur. All of the minus modes approach the corresponding plus modes under a simulated melting (f_H approaches 0). This slight softening is especially prominent for the low-lying Raman modes and the 110- and 144-cm^{-1} minus ξ modes [see Fig. 9(a)].

When examining the eigenvectors in Table IV, note that the mass difference of adenine and thymine causes the absolute value of the amplitudes of corresponding subunits in the two chains to be different. It is noteworthy that the general character of the eigenvectors, of the optical modes for vibrations in the ζ direction, is very similar to that of corresponding modes in the ξ and η directions.

The oscillator strengths S_j of the observed IR-active modes in polycrystalline poly(dA)·poly(dT) below 110 cm^{-1} were obtained from experiment (Fig. 5) by applying a multioscillator fit using (1). The constants obtained from this fit are listed in Table V. In the Appendix we derive an expression for the oscillator strengths S_j for $\theta=0$ modes and describe how to obtain S_j at $\pi/5$ within our ladder model. For the evaluation of this expression we use our calculated eigenvectors and a charge distribu-

TABLE IV. Eigenfrequencies and eigenvectors of zone center, ζ modes. Eigenfrequencies are labeled ν_a, ν_b, ν_c, and ν_d according to increasing frequency, respectively (see text). For the plus modes the eigenvector of ν_a has been omitted because it is the translation of the whole chain. The numbers of this table are based on the parameters of Table III.

Eigenfrequency (cm^{-1})	ν_b^+ 63	ν_c^+ 83	ν_d^+ 170	ν_a^- 15	ν_b^- 65	ν_c^- 86	ν_d^- 171
Na_1	6.79	−1.96	−0.19	1.05	11.08	−1.70	−0.19
P_1	1	1	1	1	1	1	1
S_1	0.09	0.68	−1.44	0.98	−0.35	0.62	−1.44
A	−1.93	−0.79	0.22	0.88	−3.02	−0.94	0.24
T	−1.25	−0.38	0.32	−0.91	4.78	2.00	−1.60
S_2	0.06	0.33	−0.21	−1.00	0.56	−1.32	9.73
P_2	0.65	0.48	0.15	−1.03	−1.58	−2.13	−6.76
Na_2	4.41	−0.95	−0.03	−1.08	−17.52	3.62	1.27

TABLE V. Oscillator-fit for the IR data of Na-poly(dA)·poly(dT).

Frequency[a] (cm^{-1})	Oscillator[b] strength	$T=7$ K Full width[c] half height (cm^{-1})	Extinction[d] coefficient	Index of[e] refraction
63	0.100	6.8	0.243	1.91
83	0.028	3.3	0.200	1.88
86	0.008	2.2	0.145	1.78
100	0.012	3.3	0.104	1.83
110	0.002	2.2	0.040	1.82

[a]Frequencies are known to within ± 0.3 cm^{-1}.
[b]Oscillator strengths are known to within $\pm 10\%$, with the exception of the 110 cm^{-1} which is $\pm 20\%$.
[c]Widths are known to within ± 0.3 cm^{-1}.
[d]Extinction coefficients are known to within ± 0.01.
[e]Indices of refraction are known to within 0.5%.

TABLE VI. Charge distribution on Na-poly(dA)·poly(dT) and calculated oscillator strengths.

			Charge on DNA subunits[a]				
Na^+	PO_4^-	d-Ribose	Adenine	Thymine	d-Ribose	PO_4^-	Na^+
1	−1.34	0.49	−0.22	−0.04	0.45	−1.340	1

	Calculated oscillator strengths[b]					
	ξ modes ($\theta=0$)		ξ modes ($\theta=\pi/5$)		η modes ($\theta=\pi/5$)	
Normal modes[c]	Eigenfrequency (cm^{-1})	Oscillator strength	Eigenfrequency (cm^{-1})	Oscillator strength	Eigenfrequency (cm^{-1})	Oscillator strength
ν_b^+	63	0.152	100	0.016	86	0.008
ν_c^+	83	0.104	140	0.028	126	0.024
ν_d^+	170	0.013	238	0.005	220	0.004
ν_b^-	65	0.007	110	0.000 09	88	0.002
ν_c^-	86	0.013	144	0.0009	126	0.014
ν_d^-	171	0.006	239	0.0006	220	0.003

[a]In units of electronic charge e.
[b]The three acoustic modes are omitted from this table because the motion at zone center is only uniform translation which has no dipole moment. The two Raman modes are omitted since their dipole moment is essentially zero.
[c]Normal modes are labeled ν_b, ν_c, and ν_d according to increasing values and + and − superscripts indicate plus and minus modes, respectively.

tion on the subunits of our model, which is close to the σ and π charge distribution given by Renugopalakrishnan *et al.*[44] We alter that distribution slightly to maintain the charge neutrality which is required for a solid sample. We do not try to take into account any polarizability of the subunits in order to obtain dynamical effective charges because of the complexity of the problem.

The results of the oscillator strength calculations are shown in Table VI. The S_j values for the 63-, 83-, 86-, and 100-cm^{-1} modes match well with the corresponding experimental values in Table V. However, the model yields an oscillator strength for the 110-cm^{-1} mode which is about two orders of magnitude too small. Mass asymmetry between the two chains of the model plays a very influential role in the calculation of oscillator strength of the minus modes, whereas it hardly affects the plus modes. An additional mass difference between bases of two water molecules (on the adenine for example) brings the S of the 110-cm^{-1} mode up to a reasonable value of 0.004 and causes a typical decrease for a plus mode of 15%.

We begin the discussion of our experimental results by noting that the spectra of poly(dG)·poly(dC) in Figs. 1 and 2 illustrate two points which apply to all of the samples we measured, the origin of the sharp 170-cm^{-1} line and the effect of temperature on spectra. A comparison of the solid and short-dashed traces in Fig. 1 indicates that the very intense line at 170 cm^{-1} occurs only in the saturated salt case in which small NaCl crystals are present. The IR absorption of small NaCl crystals is near 171 cm^{-1} at 290 K in vacuum but it shifts slightly downwards if it is immersed in a medium with a higher dielectric constant such as DNA.[45] Therefore, the absorption at 170 cm^{-1} in saturated salt films is mainly assigned to small NaCl crystals. However, it must be pointed out that this assignment does not exclude the possibility of DNA lattice modes absorbing at this frequency. In fact minimal salt poly(dA)·poly(dT) appears to have a band near this frequency (Fig. 6).

Since the effect of low temperature is most likely the freezing out of the multiphonon difference processes,[46] it is reasonable to expect that spectra taken at low tempera

tures will have lower overall absorption. This fact is demonstrated by comparing the 5 and 300 K curves for poly(dG)·poly(dC) (Fig. 1). Both curves were obtained by measuring the same film. At 5 K we find a smaller extinction coefficient than at 300 K across the entire spectrum. Similar effects occur for all our samples at all frequencies.

The spectral features around 60 cm^{-1} occurring in all of the poly(dG)·poly(dC) samples (Figs. 1 and 2) are asymmetric in such a way that the high-frequency side has an increased width. In particular, the solid curve in Fig. 2 shows a pronounced shoulder at 74 cm^{-1} which might be the mode corresponding to the 83 cm^{-1} in poly(dA)·poly(dT) since its frequency ratio to the 56 cm^{-1} is the same as the frequency ratio of the 83- to the 63-cm^{-1} modes. In fact, the lattice-dynamical model shows that such a mode should also exist for poly(dG)·poly(dC).

The bands in Figs. 1 and 2 which are characteristic of poly(dG)·poly(dC) are located at 230 and 400 cm^{-1}. Additionally, the weak bands of poly(dG)·poly(dC) at 142 and 181 cm^{-1} in Fig. 2 are reminiscent of the 140- and 170-cm^{-1} modes in the lattice-dynamical model of poly(dA)·poly(dT) (Fig. 8).

The structural information available concerning poly(dG)·poly(dC) indicates that sequences of guanine stabilize the *A* conformation.[47] Since this homopolymer has never been observed in the *Z* conformation[48] and our measurements were performed at low humidities it is plausible that the poly(dG)·poly(dC) spectra of Figs. 1 and 2 are characteristic of *A*-form DNA.

In all of our measurements on polynucleotides and natural DNA we found a pronounced and broad absorption minimum around 300 cm^{-1}. The same observation has been made by Beetz and Ascarelli[10] on RNA samples. To reiterate, they assigned the observed modes above this broad minimum to ribose ring vibrations, i.e., "inner vibrations" (vibrations within the subunits). This means that the 300-cm^{-1} minimum separates the main outer modes from the inner modes.

The spectrum of poly(dA-dT)·poly(dA-dT) in Fig. 2 has characteristic bands at 195, 350, and 420 cm^{-1}.

A low-temperature FIR spectrum of poly(rA)·poly(rU) is shown in Fig. 3. The band at 40 cm^{-1} and the shoulder at 56 cm^{-1} are again considered as the two low-frequency modes corresponding to those modes previously mentioned for the other polynucleotides.

Figure 6 shows the detailed structure of the polycrystalline poly(dA)·poly(dT) film above 110 cm^{-1} and also the effect of salt. One outstanding aspect of Fig. 6 is that the oscillator strength across the entire spectrum is much lower for the salted film. We suggest that neutralization of the subunit charges by the Na^+ and Cl^- ions may be responsible. Very recently Jenkins *et al.*[49] have reported the binding of a cation Cs^+ to adenine and thymine bases. Similar Na^+ binding might be expected to have the effect shown in Fig. 6 of reducing oscillator strength. Additionally, the masses of Na^+ and Cl^- ions would affect the lattice dynamics if they were attached to the molecular subunits. Generally speaking the addition of ionic mass to the DNA molecule in a nonperiodic fashion would smear out the modes, which is the case for the dashed curve in Fig. 6. Comparing the background in Figs. 5 and 6 one sees that the large excess in Fig. 6 at low frequencies is absent in Fig. 5 and is therefore likely due to a phenomenon which freezes out at low temperatures. The remaining temperature-independent background in Fig. 5 may be disorder induced one phonon absorption due to that part of the sample which is amorphous.[50,51]

V. CONCLUSIONS

Far-infrared absorption measurements (40—500 cm^{-1}) on films of sequence-defined polydeoxyribonucleotides poly(dA)·poly(dT), poly(dA-dT)·poly(dA-dT), and poly(dG)·poly(dC), and the polyribonucleotide poly(rA)·poly(rU) presented here reveal a considerable amount of hitherto unpublished information concerning DNA dynamics. We have measured the spectral dependence on temperature and NaCl content. Highly polycrystalline, double helical, minimal salt poly(dA)·poly(dT) showed four sharp bands at 63, 83, 100, and 110 cm^{-1} when measured at 7 K. These modes are not resolved in poly(dG)·poly(dC) spectra, but a shoulder on the 56-cm^{-1} peak indicates the existence of the mode corresponding to the 83-cm^{-1} mode in poly(dA)·poly(dT). Additionally, minimal salt poly(dA)·poly(dT) has a detailed spectrum of "outer" modes up to 250 cm^{-1}. We have discussed these experimental results along with Brillouin scattering and low-frequency Raman observations in terms of a lattice-dynamical model of an unraveled poly(dA)·poly(dT) duplex which is designed to explain only the modes with extended displacement fields. Using the eigenvectors resulting from this calculation and assuming a charge distribution, we have calculated the oscillator strengths of the low-lying FIR modes and found that these values compared favorably with the values extracted from the measurements presented here.

A sharp and intense feature near 170 cm^{-1} occurs in all types of DNA films which have been dialyzed against saturated salt solutions and therefore this feature is assigned largely to absorption by small NaCl crystals.

We have shown that small amounts of salt can severely broaden bands and even decrease oscillator strengths. Additionally, it has become clear that the extent of polycrystallinity plays an important role in allowing the IR-active modes of nucleic acid modes to be observed.

ACKNOWLEDGMENTS

J.W.P., G.S.E., and A.W. express their thanks to the Max-Planck-Gesellschaft zur Förderung der Wissenschaften (München, Germany) for financial support. We appreciate the helpful suggestions and critical comments of Dr. W. Kress. We thank Dr. A. Poglitsch and Dr. G. Bechtold for their programming assistance. We are grateful to Mr. W. König for helping with the FIR spectroscopy. We thank Dr. S. M. Lindsay and co-workers for making their manuscripts available before publication. G.S.E. thanks the U.S. Office of Naval Research (Arlington, VA) for its support under Grant No. N00014-85-G-0188.

APPENDIX

In order to derive an expression for the dielectric oscillator strength we consider the contribution to the dielectric function in a direction w (ξ, η, or ζ) of a vibrational chain mode j of our model (Fig. 7) in an oriented sample by taking into account only diagonal terms of the dielectric tensor[52]

$$\Delta\epsilon_j=\frac{4\pi}{s_h v_c}\frac{\left[\sum_{s=1}^{s_h}\sum_{\kappa} q_\kappa m_\kappa^{-1/2} e_w(s,\kappa;j)\right]^2\cos^2\phi}{\omega_j^2-\omega^2-i\omega\gamma_j} . \tag{A1}$$

ϕ is the angle of the resulting dipole moment of mode j with respect to the existing field. v_c (c representing cell) is the volume of the nucleotide unit cell of the chain. s labels unit cells, s_h is the upper limit of the s sum (for brevity the limits on the sum are implied in further equations), and m_κ and q_κ represent the mass and dynamical charge of the κth particle in the nucleotide unit cell, respectively. e_w is the w component of the eigenvector of mode j. We consider the following two cases for s: first $\theta=0$ for the ζ modes, and second $\theta=\pi/5$ for the ξ and η modes. In the former case we set $s_h=1$ in Eq. (A1) and the sum has only one term. In the second case $s_h=10$, i.e., the number of base pairs in the helix period. The eigenvector $e(s,\kappa;j)$ is normalized as

$$\sum_s\sum_\kappa e_w(s,\kappa;j)^2=1 . \tag{A2}$$

If we represent the actual displacement described in the reference frame fixed to the molecule of particle (s,κ) in mode j by $w(s,\kappa;j)$ and use mass-weighted coordinates such that $e_w\sim m^{1/2}\cdot w$ we find, with the help of Eq. (A2), that

$$e_w(s,\kappa;j)=\frac{m_\kappa^{1/2}w(s,\kappa;j)}{\left[\sum_{s'}\sum_{\kappa'} m_{\kappa'}w(s',\kappa';j)^2\right]^{1/2}} . \tag{A3}$$

If we adopt the conventional definition of the dielectric oscillator strength S_j, then the contribution of the mode j to the dielectric function can then be written as

$$\Delta\epsilon_j=\frac{S_j\omega_j^2}{\omega_j^2-\omega^2-i\omega\gamma_j} . \tag{A4}$$

Equations (A1) and (A3) yield the expression for dielectric oscillator strength:

$$S_j=\frac{1}{3}\frac{4\pi}{v_c s_h}\frac{\left[\sum_s\sum_\kappa q_\kappa w(s,\kappa;j)\right]^2}{\sum_s\sum_\kappa m_\kappa w(s,\kappa;j)^2\omega_j^2} . \tag{A5}$$

The factor of $\frac{1}{3}$ arises because of spatial averaging over the $\cos^2\phi$ term for a sample of unoriented chains. The physical interpretation of this expression is that the dielectric oscillator strength is proportional to the ratio of the polarization energy to the mechanical energy of the mode j.

For the case of our ζ modes Eq. (A5) becomes

$$S_j=\frac{1}{3}\frac{4\pi}{v_c}\frac{\left[\sum_\kappa q_\kappa\zeta(\kappa;j)\right]^2}{\sum_\kappa m_\kappa[\zeta(\kappa;j)]^2\omega_j^2} . \tag{A6}$$

The second case concerns the transverse motions ξ and η. For these modes the unit cell contains ten nucleotide pairs along the helix axis. Such displacements have a dielectric oscillator strength only at $\theta=\pi/5$ in our model (we considered the base-pair plane to be perpendicular to the helix axis). The denominator of Eq. (A5) is proportional to the mechanical energy of mode j. Therefore the w's occurring there are just those coming from our calculation. The displacement w in the numerator of Eq. (A5) must now be reinterpreted as the projection of the ladder w's into the helical configuration where they yield now a nonzero dipole moment. In this manner we can simulate the screw symmetry of the real helix by using the lattice dynamics of the unraveled model.

It should be noted here that the unraveled ladder model fails to describe the acoustic branches at $\theta=\pi/5$ for the ξ and η modes if projected into the helical configuration. In fact, the branches should go to zero at this point, corresponding to a translation of the DNA duplexes perpendicular to its axis. Additionally, since the model does not consider torsional motions it has $3N$-3 optical branches instead of the required $3N$-4 (where N is the number of particles in the unit cell). The lowest-lying η^- mode is most likely that which would become torsional in a model which accounts for rotational degrees of freedom, since its eigenvector and eigenfrequency most closely resemble torsional motions.

*Present address: Department of Physics and Astronomy, Vanderbilt University, Nashville, TN 37235.

†Present address: Max-Planck-Institut für Polymerforschung, Postfach 3148, D-6500 Mainz, Federal Republic of Germany.

‡On leave of absence from Instytut Fizyki, Polskiej Akademii Nauk (IFPAN) Aleja Lotników 32/46, PL-02-668 Warszawa, Poland.

[1]S. M. Lindsay, J. W. Powell, E. W. Prohofsky, and K. V. Devi-Prasad, in *Structure and Dynamics of Nucleic Acids, Proteins and Membranes,* edited by E. Clementi, G. Corongiu, M. H. Sarma, and R. H. Sarma (Adenine, New York, 1984), p. 531; J. M. Eyster and E. W. Prohofsky, Phys. Rev. Lett. **38**, 371 (1977); W. N. Mei, M. Kohli, E. W. Prohofsky, and L. L. Van Zandt, Biopolymers **20**, 833 (1981); Y. Kim and E. W. Prohofsky, Phys. Rev. B **33**, 5676 (1986).

[2]M. Levitt, Cold Spring Harbor Symp. Quant. Biol. **46A**, 251 (1982).

[3]B. Tidor, K. I. Irikura, B. R. Brooks, and M. Karplus, J. Biomol. Struct. Dyn. **1**, 231 (1983).

[4]J. A. Krumhansl, G. M. Wysin, D. M. Alexander, A. Garcia, P. S. Lohmdahl, and S. P. Layne, in *Structure and Motion: Membranes, Nucleic Acides and Proteins,* edited by E. Clementi, G. Corongiu, M. H. Sarma, and R. H. Sarma (Adenine, New York, 1985), p. 407.

[5]A. Scott, Phys. Rev. A **31**, 3518 (1985).
[6]J. M. Eyster and E. W. Prohofsky, Biopolymers **13**, 2505 (1974).
[7]J. M. Eyster and E. W. Prohofsky, Biopolymers **13**, 2527 (1974).
[8]G. Maret, R. Oldenbourg, G. Winterling, K. Dransfeld, and A. Rupprecht, Colloid Polym. Sci. **257**, 1017 (1979).
[9]M. B. Hakim, S. M. Lindsay, and J. Powell, Biopolymers **23**, 1185 (1984).
[10]C. P. Beetz, Jr., and G. Ascarelli, Biopolymers **21**, 1569 (1982); **15**, 2299 (1976); Spectrochimia Acta Part A **36**, 299 (1980); **36**, 525 (1980).
[11]A. Wittlin, L. Genzel, F. Kremer, S. Häseler, A. Poglitsch, and A. Rupprecht, Phys. Rev. A **34**, 493 (1986).
[12]G. S. Edwards, C. C. Davis, J. D. Saffer, and M. L. Swicord, Phys. Rev. Lett. **53**, 1284 (1984); Biophys. J. **47**, 799 (1985).
[13]M. Kohli, N. Mei, E. W. Prohofsky, and L. L. Van Zandt, Biopolymers **20**, 853 (1981).
[14]B. H. Dorfman and L. L. Van Zandt, Biopolymers **22**, 2639 (1983).
[15]L. L. Van Zandt, Int. J. Quantum Chem., Quantum Biol. Symp. **8**, 271 (1981).
[16]L. L. Van Zandt, Phys. Rev. Lett. **57**, 2085 (1986).
[17]S. M. Lindsay and J. Powell, Biopolymers **22**, 2045 (1983).
[18]B. F. Putnum, L. L. Van Zandt, E. W. Prohofsky, and W. N. Mei, Biophys. J. **35**, 271 (1981).
[19]J. M. Eyster and E. W. Prohofsky, Biopolymers **16**, 965 (1977).
[20]A. J. Martin, Biopolymers **23**, 471 (1984).
[21]P. C. Painter, L. Mosher, and C. Rhoads, Biopolymers **20**, 243 (1981).
[22]C. DeMarco, S. M. Lindsay, M. Porkorny, and J. Powell, Biopolymers **24**, 2035 (1985).
[23]H. Urabe and Y. Tominaga, Biopolymers **21**, 2477 (1982).
[24]S. M. Lindsay, J. W. Powell, and A. Rupprecht, Phys. Rev. Lett. **53**, 1853 (1984).
[25]S. M. Lindsay, in *Progress and Challenges in Biological and Synthetic Polymer Research,* edited by C. Kawabata and A. R. Bishop (Ohmska, Tokyo, 1986).
[26]Y. Tominaga, M. Shida, K. Kubota, H. Urabe, Y. Nishimura, and M. Tsuboi, J. Chem. Phys. **83**, 5972 (1986).
[27]N. J. Tao, S. M. Lindsay, and A. Rupprecht (private communication).
[28]S. A. Lee, S. M. Lindsay, J. W. Powell, T. Weidlich, N. J. Tao, G. D. Lewen, and A. Rupprecht (private communication).
[29]W. Saenger, *Principles of Nucleic Acid Structure* (Springer, Berlin, 1984).
[30]S. Arnott, R. Chandrasekharan, I. H. Hall, and L. C. Puigjaneer, Nucleic Acid Res. **11**, 4141 (1983).
[31]G. A. Thomas and W. L. Peticolas, J. Am. Chem. Soc. **105**, 993 (1983).
[32]B. Jollès, L. A. Laigle, L. Chinsky, and P. Y. Turpin, Nucleic Acid Res. **13**, 2075 (1985).
[33]S. Arnott and E. Selsing, J. Mol. Biol. **88**, 2527 (1974).
[34]C. R. Cantor, M. M. Warshaw, and H. Shapiro, Biopolymers **9**, 1059 (1970).
[35]R. M. Wartell and J. T. Harrell, Biochemistry **25**, 2664 (1986).
[36]S. Diekmann FEBS Lett. **195**, 53 (1986).
[37]H.-S. Koo, H.-M. Wu, and D. Crothers, Nature **320**, 501 (1986).
[38]H.-M. Wu and D. Crothers, Nature **308**, 509 (1984).
[39]P. L. Hagerman, Nature **321**, 449 (1986).
[40]A. Rupprecht and B. Forslind, Biochem. Biophys. Acta **204**, 304 (1970).
[41]L. Genzel, A. Poglitsch, and S. Häseler, Int. J. Infrared Millimeter Waves **6**, 741 (1985).
[42]E. E. Bell, in *Light and Matter Ia,* Vol. XXV/2a of *Encyclopedia of Physics,* edited by S. Flügge and L. Genzel (Springer, Berlin, 1967).
[43]H. Urabe and Y. Tominaga, J. Phys. Soc. Jpn. **50**, 3543 (1981).
[44]U. Renugopalakrishnan, A. Lakshminarayanan, and V. Sasiesekharan, Biopolymers **10**, 1159 (1971).
[45]L. Genzel and T. P. Martin, Surf. Sci. **34**, 33 (1973).
[46]H. Bilz, D. Strauch, and R. K. Wehner, in *Light and Matter Id,* Vol. XXV/2d of *Encyclopedia of Physics,* edited by S. Flügge and L. Genzel (Springer, Berlin, 1984).
[47]Y. Nishimura, C. Torigoe, and M. Tsuboi, Biopolymers **24**, 1841 (1985).
[48]R. Santella, D. Grunberger, I. B. Einstein, and A. Rich, Proc. Nat. Acad. Sci. U.S.A. **78**, 1451 (1981).
[49]B. G. Jenkins, R. M. Wartell, and J. L. Aldever, Biopolymers **25**, 823 (1986).
[50]A. S. Barker and A. J. Sievers, Rev. Mod. Phys. **47**, Suppl. 2, S1 (1975).
[51]L. Genzel, in *Optical Properties of Solids,* edited by S. Nudelman and S. S. Mitra (Plenum, New York, 1969), Chap. 15.
[52]M. Born and K. Huang, *The Dynamical Theory of Crystal Lattices* (Clarendon, Oxford, 1968), p. 340.